Dense wavelength conversion and multicasting in a resonance-split silicon microring

Qiang Li,[1] Ziyang Zhang,[2] Fangfei Liu,[1] Min Qiu,[2,a)] and Yikai Su[1,b)]

[1]State Ke Lab at of Ad a ced O tical C mm icati S tem a d Netw k ,
De a tme t f Elect ic E gi ee i g, Sha ghai Jia T g U e it , Sha ghai 200240, Chi a
[2]Lab at f O tic , Ph t ic a d Q a t m Elect ic , De a tme t f Mic elect ic a d A lied
Ph ic , R al I tit te f Tech l g (KTH), Elect m 229, 164 40 Ki ta, Swede

We experimentally demonstrate all-optical wavelength conversions in a 10 μm radius resonance-split silicon microring resonator based on free carrier dispersion effect. The split resonance is caused by the mutual coupling between the two countertraveling modes inside the ring resonator. Dense wavelength conversions are performed at data rates from 500 Mbytes/s to 5 Gbytes/s and a dual-channel wavelength multicasting is realized at a data rate of 1.25 Gbytes/s. The resonance splitting phenomenon opens up opportunities to convert more closely spaced wavelengths, thus effectively increasing the system capacity. © 2008 Ame ica I tit te f Ph ic .
[DOI: 10.1063/1.2976123]

Wavelength conversion is an important function for all-optical networks to alleviate the data blocking due to wavelength contention in the dynamic, high-capacity wavelength-division-multiplexed (WDM) networks.[1] The all-optical wavelength converter is regarded as a promising alternative to optical-electronic-optical wavelength conversion.[2] It has been demonstrated in a variety of media, such as highly nonlinear fibers,[3] semiconductor optical amplifiers,[4] periodically poled lithium niobate crystals,[5] and GaAs microring resonators.[6] Recently, silicon-on-insulator (SOI) nanophotonic waveguides, i.e., silicon wires, have attracted much attention due to their compact sizes and compatibility with the complementary metal oxide semiconductor fabrication. The wavelength conversions have been demonstrated in silicon straight waveguides by exploiting four-wave mixing[7,8] and in silicon ring resonators based on the free carrier dispersion (FCD) effect and resonance shift.[9] The use of a microring resonator with a high quality factor can compensate the weak nonlinearity of the miniaturized silicon devices and thus relax the power requirement.

For the wavelength conversion based on the FCD effect in a silicon ring resonator, a pump light and a signal light are required, where they work at different resonances. The signal light is usually a continuous wave (cw). In the previous reports, however, the pump and signal resonances are separated by at least one free space range (FSR).[9] For the small-radius ring resonator in SOI, the FSR is usually large, thus limiting the choices of wavelengths/channels that can be adopted for the conversion. A conventional microring with a FSR below 1 nm requires a diameter of a few 100 μm.[10] For a ring resonator side coupled to a waveguide, if periodic roughness (grating) on the sidewall of the ring is introduced, both propagating and counterpropagating modes can be excited.[11] The induced resonance splitting eliminates the need of separating the pump and signal by at least a FSR and enables more channels for conversions, thus significantly increasing the system capacity. In this paper, we demonstrate

high-speed dense wavelength conversion and dual-channel wavelength multicasting, based on the FCD effect in the resonance-split silicon microring resonator.

As shown in Ref. 11, the resonance splitting is caused by the mutual coupling between the modes inside the ring resonator. The incident wave s_i only generates the counterclockwise traveling mode a, which in turn induces the counterpropagating mode b due to the grating that is present along the ring sidewalls, as shown in Fig. 1. Modes a and b are related by the mutual coupling factor Q. Considering the degenerate case, modes a and b have the same resonance frequency ω_0, intrinsic quality factor Q_i, and coupling quality factor Q_e. The transmission function of the ring resonator is given by

$$\frac{s_t}{s_i} = 1 - \frac{\omega_0}{2Q_e}\left[\frac{1}{j\left(\omega - \omega_0 + \frac{\omega_0}{2Q}\right) + \frac{\omega_0}{2Q_i} + \frac{\omega_0}{2Q_e}} + \frac{1}{j\left(\omega - \omega_0 - \frac{\omega_0}{2Q}\right) + \frac{\omega_0}{2Q_i} + \frac{\omega_0}{2Q_e}}\right].$$

It can be seen that mode a is split into two resonance frequencies, namely, $\omega_0 - \omega_0/(2Q)$ and $\omega_0 + \omega_0/(2Q)$. Therefore, the splitting separation is solely determined by the mutual coupling factor Q.

The microring resonator used in the experiments is fabricated on a commercial single-crystalline SOI wafer with a 250-nm-thick silicon slab on top of a 3 μm silica buffer layer. The radius of the ring is 10 μm. The ring/waveguide cross section is 450×250 nm^2 with an effective area of

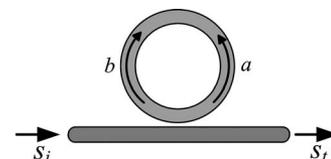

FIG. 1. Schematic of a ring resonator side coupled to a waveguide.

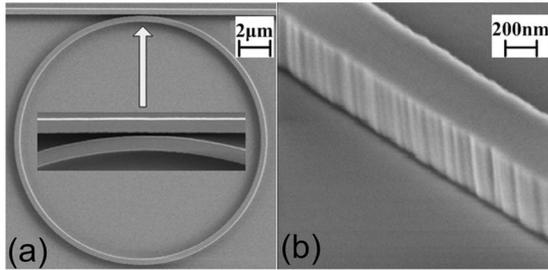a)Electronic mail: min@kth.se.
b)Electronic mail: yikaisu@sjtu.edu.cn.

FIG. 2. The SEM photos of (a) the silicon microring resonator with a radius of 10 μm and (b) the grating on the sidewall of the ring resonator. Inset in (a) is a zoom-in view of the coupling region.

about 0.1 μm^2 for the transverse-electric (TE) mode. The microring is side coupled to the straight waveguide with an air gap of 120 nm. The waveguide and ring patterns are first defined in the e-beam lithography and transferred to the top silicon layer by reactive ion plasma etching. The waveguide is slowly tapered to a width of 10 μm at both ends, where gold gratings are added to couple light near vertically from single mode fibers.[12] The grating couples only TE light with a minimal fiber-to-fiber loss below 20 dB. The scanning electron microscope (SEM) photo of the silicon microring resonator is provided in Fig. 2(a). Figure 2(b) shows the grating on the ring sidewall. The width of the grating ridge is ~20 nm and the period ranges from ~50 to ~100 nm. They are determined by a variety of parameters during the e-beam process, namely, the scan step size, line scan intervals, exposure dose, and developing time, which have been detailed in Ref. 11.

Figure 3 shows the spectral response of the ring resonator. The notches around 1550 nm are fitted using Eq. (1). The obtained intrinsic Q_i, coupling Q_e, and mutual coupling Q are 6.5×10^4, 2.0×10^4, and 3.7×10^3, respectively, indicating a strong mutual coupling and thus resonance splitting.

The experimental setup is depicted in Fig. 4. The pump wavelength λ_1 is chosen to offset the thermal nonlinear effect. The signal wavelength λ_1 is fixed at the left resonance for the noninverted case and λ_2 at the shorter wavelength edge of the left resonance for the inverted case. A Mach–Zehnder modulator, driven by an electrical pseudorandom bit sequence signal of 2^7-1 pattern length, is used to generate non-return-to-zero signal. The pump light is boosted by a high power erbium doped fiber amplifier (EDFA) followed by an attenuator to adjust the pump power. The pump light and the signal light are combined through a 90:10 coupler and launched into the microring resonator by the vertical
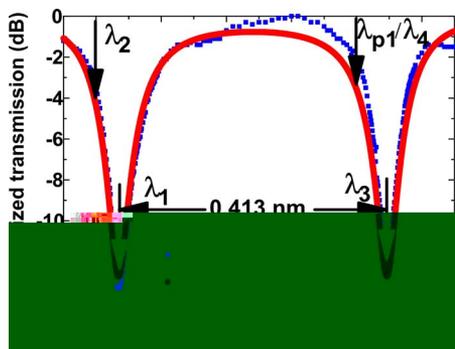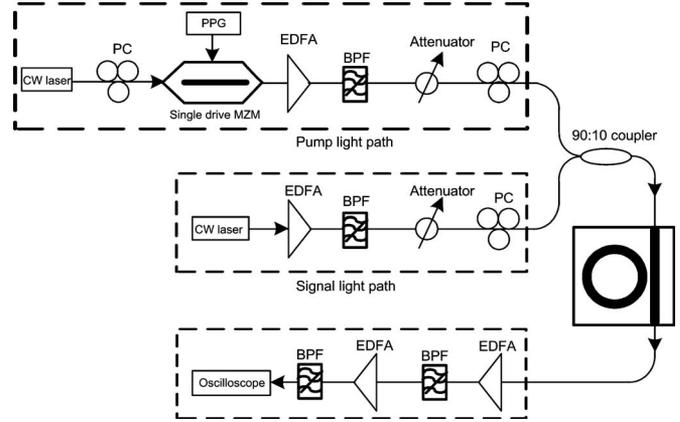

FIG. 4. Experimental setup. Pulse pattern generator.

coupling system. The output signal of the microring resonator is amplified using two cascaded EDFAs, each followed by a ~0.3 nm bandpass filter to separate the signal from the pump, and then sent to an oscilloscope to record the waveforms. As the gold grating coupler is polarization dependent, two polarization controllers are inserted before the coupler to make sure that the input pump and signal lights are in TE mode. The pump power into the input of the waveguide is ~7.7 dBm and the signal power is ~−4 dBm at the input of the fiber.

Figure 5 shows the dense wavelength conversion results

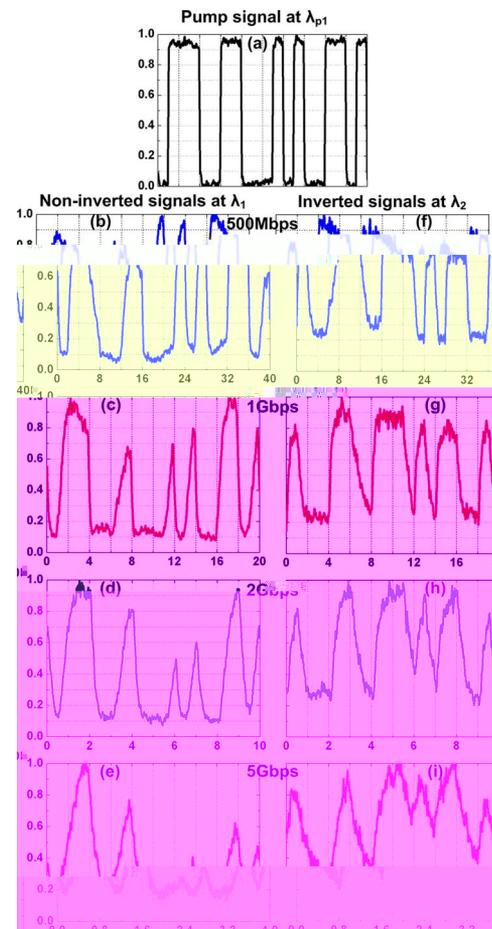FIG. 3. (Color online) The transmission spectrum demonstrating the resonance splitting effect.

FIG. 5. (Color online) Dense wavelength conversions at 500 Mbytes/s, 1 Gbyte/s, 2 Gbytes/s, and 5 Gbytes/s. The horizontal axes represent the time (ns) and the vertical axes represent the normalized intensity.
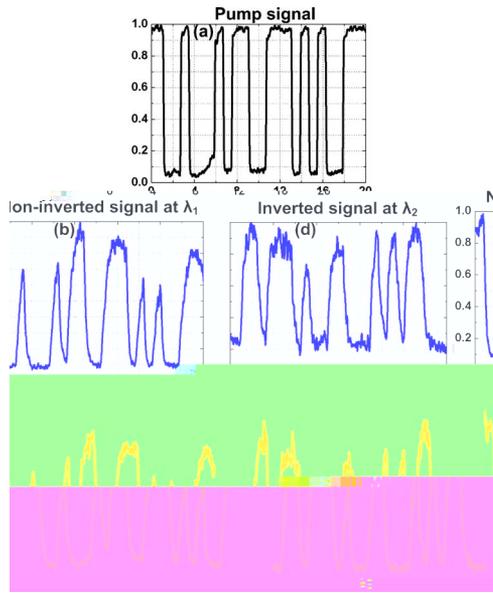
FIG. 6. (Color online) Dual-channel wavelength multicasting at 1.25 Gbytes/s. The horizontal axes represent the time (ns) and the vertical axes represent the normalized intensity.

for data rates of 500 Mbytes/s, 1 Gbyte/s, 2 Gbytes/s, and 5 Gbytes/s. Both noninverted and inverted waveforms are provided. With the signal wavelength at λ_1, the transmission of the signal light increases when the carriers are generated and the resonances are blueshifted, resulting in a noninverted conversion, as shown on the left of Fig. 5. With the signal wavelength at λ_2, the transmission of the signal light decreases when the resonances are blueshifted, resulting in an inverted conversion, shown on the right of Fig. 5. As the bit rate increases, the extinction ratio for the converted signal is reduced, mainly resulting from the long carrier lifetime.[13] The carrier lifetime induces a lower extinction ratio for the single "1's" since they have much shorter rise time and falling time compared to the consecutive 1's and thus cannot respond to the pump signal rapidly. According to the equation in Ref. 9, the resonance shift of a 3 dB bandwidth of the ring resonator corresponds to an effective index change of $\sim 1.5 \times 10^4$. The calculated required pump power is ~ 8 dBm.

We also demonstrate a dual-channel wavelength multicasting, which is needed in the WDM-based all-optical network.[14] In this process, the input signal is converted into two output wavelengths simultaneously. The locations of converted signal wavelengths are shown in Fig. 3. Another cw laser is used in this experiment and the pump is set at the resonance across a FSR ($\sim$1564 nm) with respect to the converted signal wavelength, which shows a notch depth of $\sim$25 dB and a bandwidth of $\sim$0.075 nm. Figures 6(b) and 6(c) represent the noninverted dual-channel wavelength multicasting at 1.25 Gbytes/s, while Figs. 6(d) and 6(e) demonstrate the inverted case.

For intrinsic silicon, the carrier lifetime limits the available operation speed. The carrier lifetime can be greatly reduced by using a reverse-biased *-i-* junction[15] or by ion implantation.[16,17] The pump power needed for wavelength conversion can be further reduced by fabricating ring resonators with much higher Q factors, by employing smaller radius and by improving the efficiency of the fiber-to-waveguide coupling.

To summarize, we have demonstrated the dense wavelength conversion and dual-channel wavelength multicasting in a silicon microring resonator with resonance splitting, which is caused by the mutual coupling between the two modes inside the ring. The resonance splitting in silicon microring resonators opens up opportunities to convert more wavelengths that are densely spaced and effectively increases the system capacity.

[1] S. J. B. Yoo, J. Lightwave Technol. **14**, 955 (1996).
[2] S. L. Danielsen, P. B. Hansen, and K. E. Stubkjaer, J. Lightwave Technol. **16**, 2095 (1998).
[3] K. Inoue and H. Toba, IEEE Photon. Technol. Lett. **4**, 69 (1992).
[4] T. Durhuus and B. Mikkelsen, J. Lightwave Technol. **14**, 942 (1996).
[5] J. Yamawaku, H. Takara, T. Ohara, K. Sato, A. Takada, T. Morioka, O. Tadanaga, H. Miyazawa, and M. Asobe, Electron. Lett. **39**, 1144 (2003).
[6] P. P. Absil, J. V. Hryniewicz, B. E. Little, P. S. Cho, R. A. Wilson, L. G. Joneckis, and P. T. Ho, Opt. Lett. **25**, 554 (2000).
[7] H. Rong, Y. H. Kuo, A. Liu, M. Paniccia, and O. Cohen, Opt. Express **14**, 1182 (2006).
[8] M. A. Foster, A. C. Turner, R. Salem, M. Lipson, and A. L. Gaeta, Opt. Express **15**, 12949 (2007).
[9] Q. Xu, V. R. Almeida, and M. Lipson, Opt. Lett. **30**, 2733 (2005).
[10] P. Dong, S. F. Preble, and M. Lipson, Opt. Express **15**, 9600 (2007).
[11] Z. Zhang, M. Dainese, L. Wosinski, and M. Qiu, Opt. Express **16**, 4621 (2008).
[12] S. Scheerlinck, J. Schrauwen, F. V. Laere, D. Taillaert, D. V. Thourhout, and R. Baets, Opt. Express **15**, 9625 (2007).
[13] V. R. Almeida, C. A. Barrios, R. R. Panepucci, and M. Lipson, Nature (London) **431**, 1081 (2004).
[14] R. K. Pankaj, IEEE/ACM Trans. Netw. **7**, 414 (1999).
[15] S. F. Preble, Q. Xu, B. S. Schmidt, and M. Lipson, Opt. Lett. **30**, 2891 (2005).
[16] M. Först, J. Niehusmann, T. Plötzing, J. Bolten, T. Wahlbrink, C. Moormann, and H. Kurz, Opt. Lett. **32**, 2046 (2007).
[17] M. Waldow, T. Plötzing, M. Gottheil, M. Först, J. Bolten, T. Wahlbrink, and H. Kurz, Opt. Express **16**, 7693 (2008).